




Article

# Magnetic Properties of All-*d* Metallic Heusler Compounds: A First-Principles Study

Murat Tas <sup>1,†</sup> , Ersoy Şaşıoğlu <sup>2,†</sup>  and Iosif Galanakis <sup>3,\*,†</sup> <sup>1</sup> Department of Physics, Gebze Technical University, Kocaeli 41400, Turkey; murat.tas@gtu.edu.tr<sup>2</sup> Institute of Physics, Martin Luther University Halle-Wittenberg, 06120 Halle (Saale), Germany; ersoy.sasioglu@physik.uni-halle.de<sup>3</sup> Department of Materials Science, School of Natural Sciences, University of Patras, 26504 Patra, Greece

\* Correspondence: galanakis@upatras.gr

† These authors contributed equally to this work.

**Abstract:** All-*d* metallic Heusler compounds are promising materials for nanoelectronic applications. Such materials combining *3d*, *4d*, and *5d* atoms have not yet been studied. In this respect, we perform ab initio electronic structure calculations and focus on  $\text{Co}_2\text{MnZ}$ ,  $\text{Rh}_2\text{MnZ}$ , and  $\text{Ru}_2\text{MnZ}$  compounds, where Z represents transition metal atoms from groups 3B, 4B, 5B, and 6B of the periodic table. Our results demonstrate that most of these compounds exhibit a distinctive region of very low minority-spin state density at the Fermi level when crystallized in the  $L2_1$  lattice structure. The Co-based compounds follow a Slater–Pauling behavior for their total spin magnetic moments, while the Ru-based compounds consistently deviate from the predicted Slater–Pauling values. Rh-based compounds show similarities to Co-based compounds for lighter Z atoms and to Ru-based compounds for heavier Z atoms. We find that the choice of the Z element within the same periodic table column has only a minor effect on the results, except for the  $\text{Rh}_2\text{Mn}(\text{Cr}, \text{Mo}, \text{W})$  compounds. Our findings suggest that these compounds hold significant promise for applications in spintronics and magnetoelectronics.

**Keywords:** Heusler compounds; ab initio calculations; first principles; electronic structure; ferromagnetic materials; Slater–Pauling rule



**Citation:** Tas, M.; Şaşıoğlu, E.; Galanakis, I. Magnetic Properties of All-*d* Metallic Heusler Compounds: A First-Principles Study. *Magnetism* **2024**, *4*, 400–411. <https://doi.org/10.3390/magnetism4040026>

Academic Editors: Gerardo F. Goya and Lukasz Hawelek

Received: 16 September 2024

Revised: 11 November 2024

Accepted: 3 December 2024

Published: 10 December 2024



**Copyright:** © 2024 by the authors. Licensee MDPI, Basel, Switzerland. This article is an open access article distributed under the terms and conditions of the Creative Commons Attribution (CC BY) license (<https://creativecommons.org/licenses/by/4.0/>).

## 1. Introduction

In the early 20th century, German metallurgist Heusler made a notable discovery while investigating ways to enhance the electrical conductivity of steel: the novel compound  $\text{Cu}_2\text{MnAl}$  [1,2]. As the century progressed, advances in instrumentation revealed that this compound possessed a face-centered cubic (f.c.c.) lattice structure, similar to those found in semiconductors like silicon (Si) and gallium arsenide (GaAs). This lattice structure is common among a variety of intermetallic compounds, each with unique properties. These compounds, collectively known as “Heusler compounds” or “Heusler alloys” [3,4], often exhibit ferromagnetic properties with high Curie temperatures. Among the most common are the full-Heusler compounds, such as  $\text{Co}_2\text{MnSi}$ , which follow the  $X_2YZ$  formula and crystallize in the “ $L2_1$ ” structure [3,4]. When the X element has a lower valence than Y, an “XA” structure may form, where the arrangement of atoms differs from the “ $L2_1$ ” structure. These are referred to as inverse Heusler compounds.

Half-metallic magnetic Heusler compounds [5], which behave as metals for one spin direction and as semiconductors for the other, exhibit high spin polarization at the Fermi level [6], and their total spin magnetic moment (in  $\mu_B$  units) follows integer values, a phenomenon known as the Slater–Pauling rule [7]. This makes them highly attractive for spintronic and magnetoelectronic applications, where they can provide novel functionalities in electronic devices [8–12]. First-principles calculations, or ab initio methods, have been critical in understanding material properties and predicting new Heusler compounds

with customized characteristics. In recent years, comprehensive databases based on first-principles calculations have cataloged hundreds of magnetic Heusler compounds [13–20]. Oliynyk et al. [21] also employed machine learning models trained on crystallographic data to predict the synthesizability of regular and inverse Heusler alloys, leading to the successful synthesis of new Ru–Ga–X ( $X = \text{Ti} - \text{Co}$ ) Heusler alloys, which have great potential for spintronic and magnetoelectronic applications. These databases complement focused studies on a smaller subset of Heusler compounds.

In typical full-Heusler compounds, one of the atoms is a metalloid; however, in certain magnetic Heusler alloys undergoing martensitic transformations, the metalloid can be replaced by a transition metal, leading to the creation of “all-3d-metal Heusler alloys” [22–37]. A recent study examined the anomalous Hall and Nernst conductivities of ferromagnetic all-d-metal Heusler compounds [32], utilizing high-throughput screening to assess their compositional range, ground-state structures, and mechanical and thermodynamic properties. This research predicted 686 (meta-)stable compounds and linked intermetallic bonding to structural preferences between regular and inverse Heuslers, correlating these preferences with mechanical properties. The study also screened the compounds for magneto-structural transitions at finite temperatures, opening up new pathways for optimizing materials for magnetic shape memory and caloric applications. A subsequent effort expanded this work by building a database of all-*d* Heusler compounds for magneto-caloric applications [38,39].

Building on these results, we performed first-principles electronic band structure calculations on a new class of magnetic all-3d Heusler compounds, specifically  $\text{Fe}_2\text{CrZ}$  and  $\text{Co}_2\text{CrZ}$ , where *Z* is an early 3d transition metal such as Sc, Ti, or V [40]. These compounds exhibit a pseudogap and high spin polarization at the Fermi level, although their total spin magnetic moment slightly deviates from the Slater–Pauling rule [7]. Compounds like  $\text{Co}_2\text{CrTi}$  and  $\text{Co}_2\text{CrV}$  demonstrate strong magnetic properties, driven by short-range magnetic exchange interactions, with Curie temperatures well above room temperature. Even with *B2* disorder, these compounds maintain their magnetic properties, making them highly promising for spintronic and magnetoelectronic applications [40]. In a follow-up study [41], we explored the electronic and magnetic properties of  $\text{Co}_2\text{YZ}$  compounds, where *Y* and *Z* are 3d transition metals, revealing that their high spin magnetic moments further highlight their potential for spintronic and magnetoelectronic technologies.

In this study, we build on previous work with  $\text{Co}_2\text{Mn}(\text{Sc},\text{Ti},\text{V},\text{Cr})$  all-3d Heusler compounds [41] and examine the effects of substituting Co and Sc(Ti,V,Cr) atoms with 4d and 5d elements. Specifically, we investigate potential  $(\text{Co},\text{Rh} \text{ or } \text{Ru})_2\text{Mn}(\text{Sc},\text{Ti},\text{V},\text{Cr}/\text{Y},\text{Zr},\text{Nb},\text{Mo} \text{ or } \text{Lu},\text{Hf},\text{Ta},\text{W})$  compounds. The resulting electronic and magnetic properties indicate that these compounds share several promising characteristics, making them suitable for relevant technological applications.

## 2. Computational Details

Our research focuses on investigating the ground-state properties of all-*d*-metal Heusler compounds. For this, we employ the full-potential nonorthogonal local-orbital minimum-basis (FPLO) method for first-principles electronic band structure calculations, as described in Refs. [42,43]. In these calculations, we apply the generalized gradient approximation (GGA) as the exchange–correlation functional within the Perdew–Burke–Ernzerhof (PBE) parametrization [44]. This choice is well-known for yielding precise outcomes, especially when dealing with half-metallic Heusler compounds, aligning closely with experimental observations [45,46]. To ensure the accuracy of our calculations, the total energy is converged to the 10th decimal point. Furthermore, a dense grid of *k*-points, specifically a  $20 \times 20 \times 20$  grid, conforming to the Monkhorst–Pack scheme [47], is utilized for the integrals in reciprocal space.

Full-Heusler compounds, as mentioned earlier, can crystallize in either the regular  $L2_1$  or inverse  $XA$  lattice structures (see Figure 1 in Ref. [41] for a detailed illustration of the structure). What differentiates the two structures is the sequence of the atoms in the unit

cell. In the case of the regular  $L2_1$  structure, the two Co(Rh.Ru) atoms occupy equivalent sublattices with identical environments of nearest and next-nearest neighbors. In contrast, in the inverse  $XA$  structure, the two Co(Rh.Ru) atoms are no longer equivalent, leading to a different symmetry and atomic arrangement.

In the initial phase of our study, we focus on  $\text{Co}_2\text{MnZ}$  compounds, where  $Z$  is a  $3d$ ,  $4d$ , or  $5d$  transition metal, examining both the  $L2_1$  and  $XA$  lattice structures using data from the Open Quantum Materials Database (OQMD) [48–50]. The reliability of the OQMD data is confirmed by the calculated lattice constants for  $\text{Co}_2\text{Cr}$  (V, Ti, or Sc) compounds in the regular lattice, which differ by less than 1% from those obtained through total energy calculations in Ref. [40]. Table 1 compiles all the results from OQMD for these compounds. Additionally, Table 2 presents results from the OQMD database for compounds where Co is substituted by Rh or Ru, assuming only the  $L2_1$  lattice structure, as OQMD identifies this as the ground state for these materials. Both tables include the lattice constants, formation energy ( $E_{\text{form}}$ ), and hull distance ( $E_{\text{hull}}$ ) in an eV/atom. For stability,  $E_{\text{form}}$  should be negative, indicating that the formation of the compound is energetically favorable compared to the separate elemental crystals. When assuming the  $L2_1$  structure, the compounds studied either have negative formation energy or values close to zero. However, while a negative  $E_{\text{form}}$  is necessary for experimental growth, it is not sufficient on its own. The hull distance ( $E_{\text{hull}}$ ) measures the energy difference between the assumed lattice structure and the most stable phase or mixture of phases. Although none of the studied compounds is the most stable phase, in most cases, the  $L2_1$  lattice corresponds to a hull distance of less than 0.200 eV/atom, which is considered the empirical limit for experimentally growing a material in a specific lattice structure.

**Table 1.** For the Co-based Heusler compounds, we present the equilibrium lattice constant  $a_{\text{eq}}$ , the formation energy  $E_{\text{form}}$ , and the hull distance  $E_{\text{hull}}$  (all data are taken from the Open Quantum Materials Database [48–50]). Star, \*, denotes the calculated ground state in the OQMD. The last column presents the energy difference between the  $L2_1$  and the  $XA$  lattice structures as calculated in the present study.

XYZ	Structure	$a_{\text{eq}}$ (Å)	$E_{\text{form}}$ (eV/atom)	$E_{\text{hull}}$ (eV/atom)	$\Delta E^{L2_1-XA}$ (eV/f.u.)
Co <sub>2</sub> MnSc	$L2_1$ *	5.902	−0.169	0.102	−0.735
	$XA$	5.964	0.005	0.276	
Co <sub>2</sub> MnTi	$L2_1$ *	5.759	−0.289	0.010	−0.587
	$XA$	5.799	−0.154	0.144	
Co <sub>2</sub> MnV	$L2_1$	5.603	0.196	0.365	−0.143
	$XA$ *	5.669	−0.035	0.134	
Co <sub>2</sub> MnCr	$L2_1$ *	5.614	0.093	0.122	−0.216
	$XA$	5.628	0.129	0.158	
Co <sub>2</sub> MnY	$L2_1$ *	6.161	0.072	0.213	−0.749
	$XA$	6.225	0.246	0.388	
Co <sub>2</sub> MnZr	$L2_1$ *	6.004	−0.174	0.068	−0.769
	$XA$	6.040	0.005	0.247	
Co <sub>2</sub> MnNb	$L2_1$ *	5.892	−0.080	0.068	−0.534
	$XA$	5.873	0.034	0.182	
Co <sub>2</sub> MnMo	$L2_1$ *	5.805	0.078	0.138	−0.397
	$XA$	5.743	0.151	0.211	
Co <sub>2</sub> MnLu	$L2_1$ *	6.046	−0.063	0.161	−0.769
	$XA$	6.114	0.125	0.349	
Co <sub>2</sub> MnHf	$L2_1$ *	5.958	−0.250	0.037	−0.853
	$XA$	5.973	−0.050	0.237	
Co <sub>2</sub> MnTa	$L2_1$	5.807	0.181	0.401	−0.433
	$XA$ *	5.863	−0.015	0.205	
Co <sub>2</sub> MnW	$L2_1$ *	5.816	0.072	0.157	−0.390
	$XA$	5.749	0.140	0.226	

Regarding the stability of the two possible Heusler lattice structures, the second column of Table 1 marks the most stable structure for the Co-based compounds according to the OQMD with an asterisk. Except for Co<sub>2</sub>MnV and Co<sub>2</sub>MnTa, the L<sub>21</sub> structure is the most stable. We also performed our own total energy calculations, with results shown in the last column of Table 1. Negative (positive) values indicate that the L<sub>21</sub> (XA) structure is more stable. Our findings align with the OQMD, except for Co<sub>2</sub>MnV and Co<sub>2</sub>MnTa, where our calculations suggest that L<sub>21</sub> is the more stable lattice structure. For the Rh- and Ru-based compounds presented in Table 2, we report only on the L<sub>21</sub> lattice, as it is the most stable according to the OQMD, with the XA structure being significantly less stable.

**Table 2.** These data are similar to Table 1 for the Rh- and Ru-based compounds assuming only the L<sub>21</sub> lattice structure. All data are taken from the Open Quantum Materials Database [48–50].

XYZ	Structure	$a_{eq}$ (Å)	$E_{form}$ (eV/atom)	$E_{hull}$ (eV/atom)
Rh <sub>2</sub> MnSc	L <sub>21</sub>	6.258	−0.623	0.013
Rh <sub>2</sub> MnTi	L <sub>21</sub>	6.127	−0.586	0.000
Rh <sub>2</sub> MnV	L <sub>21</sub>	6.047	−0.236	0.075
Rh <sub>2</sub> MnCr	L <sub>21</sub>	6.047	−0.063	0.070
Rh <sub>2</sub> MnY	L <sub>21</sub>	6.484	−0.462	0.092
Rh <sub>2</sub> MnZr	L <sub>21</sub>	6.352	−0.576	0.011
Rh <sub>2</sub> MnNb	L <sub>21</sub>	6.236	−0.298	0.085
Rh <sub>2</sub> MnMo	L <sub>21</sub>	6.163	0.029	0.220
Rh <sub>2</sub> MnLu	L <sub>21</sub>	6.394	−0.595	0.005
Rh <sub>2</sub> MnHf	L <sub>21</sub>	6.309	−0.662	0.011
Rh <sub>2</sub> MnTa	L <sub>21</sub>	6.227	−0.375	0.091
Rh <sub>2</sub> MnW	L <sub>21</sub>	6.166	0.023	0.226
Ru <sub>2</sub> MnSc	L <sub>21</sub>	6.183	−0.187	0.103
Ru <sub>2</sub> MnTi	L <sub>21</sub>	6.065	−0.346	0.049
Ru <sub>2</sub> MnV	L <sub>21</sub>	5.984	−0.154	0.001
Ru <sub>2</sub> MnCr	L <sub>21</sub>	5.961	0.109	0.110
Ru <sub>2</sub> MnY	L <sub>21</sub>	6.414	0.077	0.306
Ru <sub>2</sub> MnZr	L <sub>21</sub>	6.292	−0.230	0.092
Ru <sub>2</sub> MnNb	L <sub>21</sub>	6.192	−0.162	0.002
Ru <sub>2</sub> MnMo	L <sub>21</sub>	6.122	0.061	0.115
Ru <sub>2</sub> MnLu	L <sub>21</sub>	6.323	−0.084	0.209
Ru <sub>2</sub> MnHf	L <sub>21</sub>	6.252	−0.328	0.079
Ru <sub>2</sub> MnTa	L <sub>21</sub>	6.187	−0.253	0.006
Ru <sub>2</sub> MnW	L <sub>21</sub>	6.139	0.004	0.069

### 3. Results and Discussion

In Ref. [40], we introduced a new class of Heusler compounds consisting exclusively of 3*d* transition metal atoms. We found that the Co<sub>2</sub>CrZ compounds were of particular interest for applications since they combined a pseudogap in the minority-spin band structure, high spin polarization at the Fermi level, high values of the spin magnetic moment, and Curie temperatures above room temperature. In a follow-up study [41], we explored the electronic and magnetic properties of Co<sub>2</sub>YZ compounds, where Y and Z are 3*d* transition metals, revealing that their substantial spin magnetic moments further highlight their potential in spintronic and magnetoelectronic technologies. In this study, we use Co<sub>2</sub>Mn(Sc,Ti,V,Cr) all-3*d* Heusler compounds as the starting point and investigate the effects of replacing Co and Sc(Ti,V,Cr) atoms with 4*d* and 5*d* elements, considerably increasing the number of all-*d* Heusler compounds with potential spintronic and magnetoelectronic applications.

#### 3.1. Electronic Properties

In the initial phase of our study, we concentrated on Co<sub>2</sub>-based compounds and performed electronic band structure calculations at their equilibrium lattice constants.

From these calculations, we derived the total density of states (DOS) per formula unit (f.u.), which is illustrated in Figure 1, along with the atom-resolved DOS shown in Figure 2. As our findings consistently indicate that the  $L2_1$  structure is the ground state, we only present results for this lattice configuration in both figures.

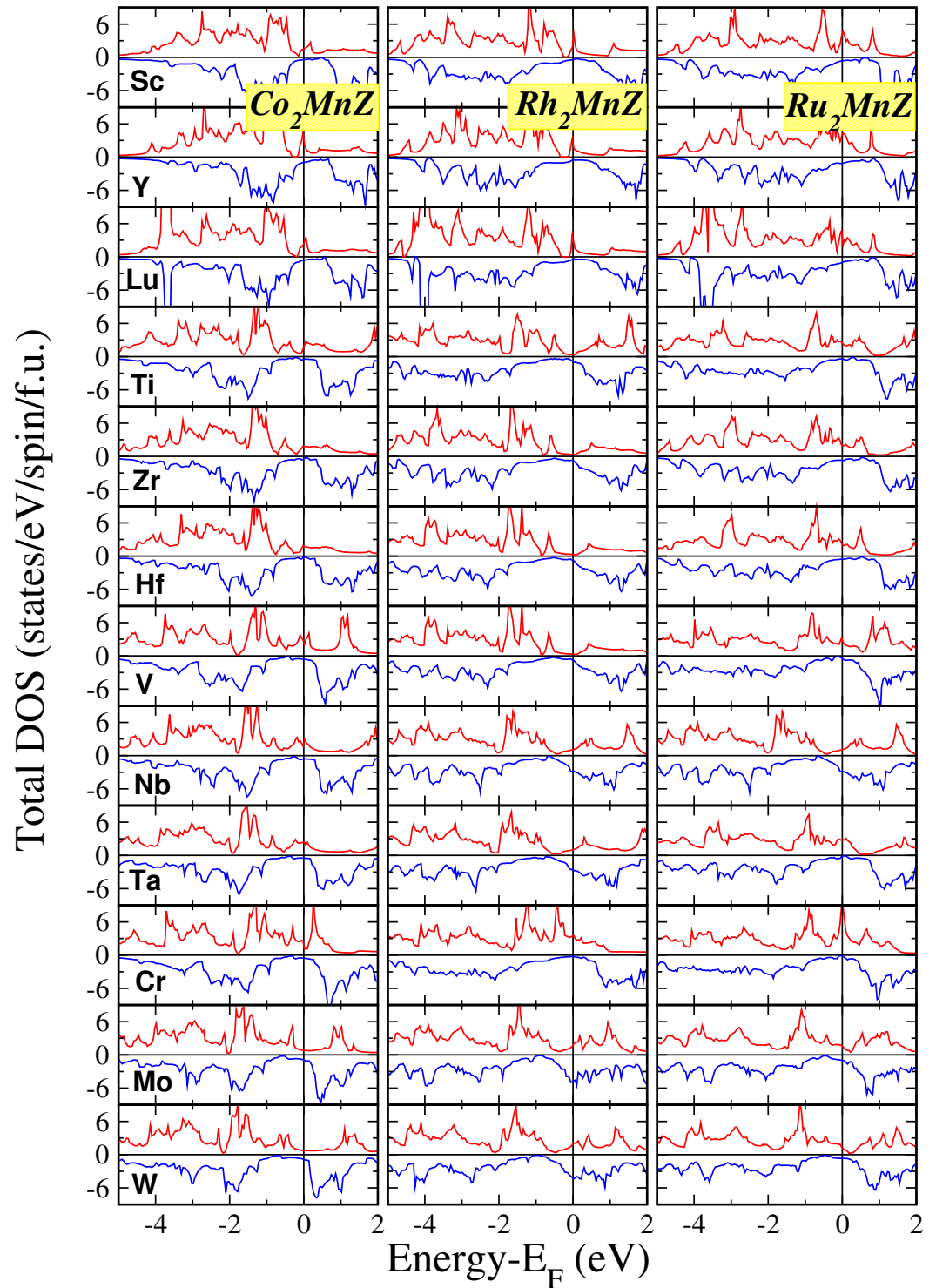


**Figure 1.** Total density of states (DOS) for all studied compounds assuming the  $L2_1$  lattice structure. Positive (negative) DOS values correspond to the majority (minority)-spin electronic band structure.

In the  $L2_1$  lattice, the total DOS displays similar features across all the compounds analyzed. A small DOS contribution at low energy, primarily from  $s$ -states, is present

but not shown in the figures. The overall DOS is largely dominated by the  $d$ -states of the transition metal atoms, with broad bands due to the high number of  $d$ -electrons in each formula unit. Specifically, the total DOS for  $\text{Co}_2\text{MnZ}$  compounds, where  $Z$  elements belong to the same column of the periodic table, shows a consistent shape, similar regions of low DOS in the spin-down channel (often referred to as the pseudogap), and the same relative positioning of the Fermi level within this pseudogap. In the atom-resolved DOS presented in Figure 2, as we move down a column of the periodic table, and the period increases, the main change occurs in the DOS of the  $Z$  atom. As expected, the width of the  $d$ -band associated with the  $Z$  atom increases, which, through hybridization, slightly broadens the  $d$ -bands of both Co and Mn atoms. However, despite these variations, the DOS remains largely consistent across all compounds, as previously noted.

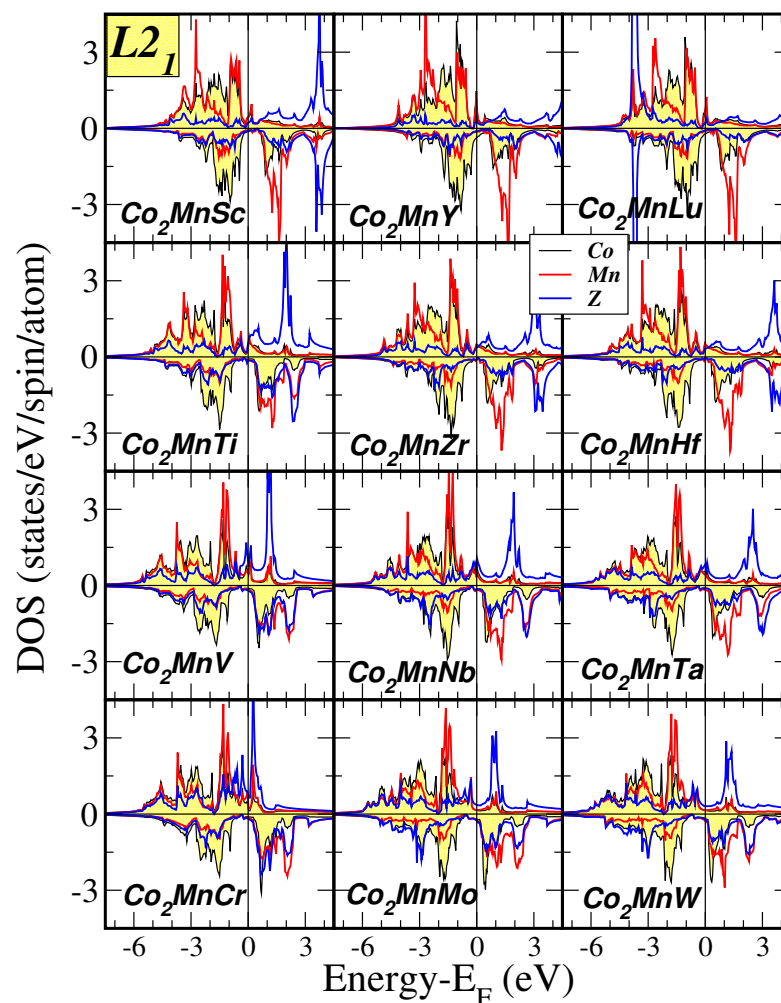


**Figure 2.** Atom-resolved DOS for the Co-based compounds assuming the  $L_{21}$  lattice. Details as in Figure 1.

In Figure 1, we also display the total DOS for all the studied Rh and Ru compounds crystallizing in the  $L_{21}$  lattice. Additionally, Figure 3 presents the atom-resolved DOS for the  $\text{RhMn}(\text{Sc}, \text{Ti}, \text{V}, \text{Cr})$  and  $\text{RuMn}(\text{Sc}, \text{Ti}, \text{V}, \text{Cr})$  compounds, compared with the corresponding Co-based compounds. When Rh replaces Co, as shown in Figure 1, the broader  $4d$  band results in less pronounced peaks and alters the shape of the spin-down pseudogap. The pseudogap itself narrows, while the DOS increases more gradually just below and above it. This trend is even more noticeable when Ru replaces Rh. The atom-resolved DOS in Figure 3 further highlights this effect. The wider  $4d$  and  $5d$  bands of Rh and Ru, compared to Co's  $3d$  band, significantly impact the DOS, particularly for the  $Z$  atoms. A notable example is observed when  $Z$  is Cr: as we progress from  $\text{Co}_2\text{MnCr}$  to  $\text{Rh}_2\text{MnCr}$  to  $\text{Ru}_2\text{MnCr}$ , the Cr majority spin

peak, which is just above the Fermi level in  $\text{Co}_2\text{MnCr}$ , shifts slightly below it for  $\text{Rh}_2\text{MnCr}$  and becomes pinned precisely at the Fermi level in  $\text{Ru}_2\text{MnCr}$ .

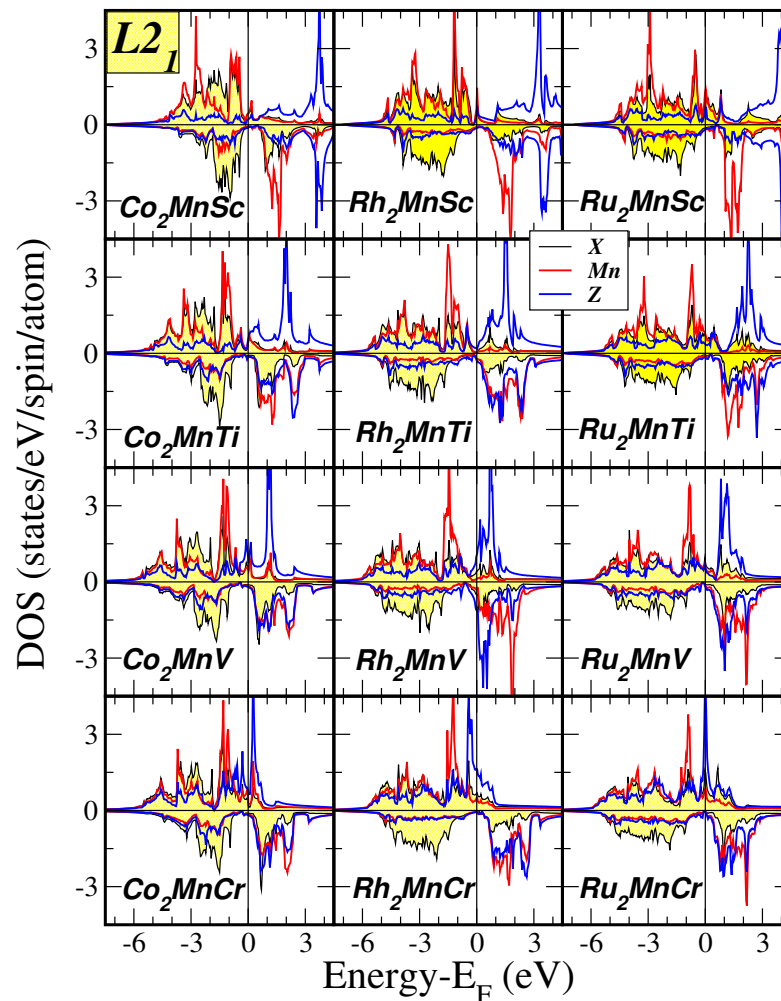


**Figure 3.** These data are similar to Figure 2 for the Co-, Rh-, and Ru-based compounds in the  $L2_1$  lattice structure when the Z atom is a 3d transition metal atom.

### 3.2. Magnetic Properties

In Table 3, we present the calculated atomic and total spin magnetic moments for all  $\text{Co}_2$  compounds investigated, based on their equilibrium lattice constants for both considered lattice structures. When a 4d element (Sc, Ti, V, Cr) is replaced by another 4d element (Y, Zr, Nb, Mo) or a 5d element (Lu, Hf, Ta, W), the magnetic properties of the compounds remain largely unchanged, with only small variations in the total spin magnetic moment within the same lattice structure and periodic table column. The spin magnetic moments of 4d atoms are smaller than those of 3d atoms, and this trend continues when substituting a 5d atom with a 4d atom. This effect is particularly notable when substituting Mo for Cr and W for Mo. Despite the changes in the atomic moments of the Z atoms, the spin moments of Co and Mn atoms are only slightly impacted, resulting in minor changes in the total spin magnetic moment. Overall, the findings from Ref. [41] concerning the total and atom-resolved spin magnetic moments in the  $L2_1$  and  $XA$  lattice structures also apply to the compounds examined in this study.

In Table 4, we present the atom-resolved and total spin magnetic moments for all compounds studied in the  $L2_1$  lattice, grouped according to their total number of valence electrons. When Rh is substituted for Co, the spin magnetic moment of Rh is significantly smaller than that of Co. This results in a more localized atomic-like behavior for the Mn spin magnetic moment, which increases to compensate for the reduction in the Rh

spin moment. Consequently, the total spin magnetic moments of both Co- and Rh-based compounds are quite similar. However, a key distinction arises for compounds with 31 valence electrons. While  $\text{Co}_2\text{MnCr}$  and  $\text{Rh}_2\text{MnCr}$  exhibit similar total spin magnetic moments, around  $7 \mu_B$ , this is not the case for  $\text{Co}_2\text{MnMo}$  and  $\text{Co}_2\text{MnW}$ . When Rh replaces Co in these compounds, the total spin magnetic moment decreases significantly. Unlike Cr, the Mo and W atoms are unable to carry substantial spin magnetic moments. The spin magnetic moment of each Rh atom is roughly  $1 \mu_B$  smaller than that of Co, and the increase in Mn's spin magnetic moment is insufficient to compensate for this decrease. Moreover, Mo and W atoms contribute little to the deficit, resulting in the total spin magnetic moment of  $\text{Rh}_2\text{MnMo}$  ( $\text{Rh}_2\text{MnW}$ ) being approximately 47% (40%) smaller than that of  $\text{Co}_2\text{MnMo}$  ( $\text{Co}_2\text{MnW}$ ). Substituting Ru for Co leads to an even greater reduction in total spin magnetic moment, as the  $5d$  states of Ru experience minimal exchange splitting, preventing Ru from carrying a significant atomic spin magnetic moment.

**Table 3.** We present the atom-resolved and total (per formula unit) spin magnetic moments for the Co-based compounds assuming both  $L2_1$  and  $XA$  lattice structures. The last column presents the total number of valence electrons in the primitive unit cell, which contains exactly one formula unit. Note that in the case of the  $XA$  lattice structure the two Co atoms are nonequivalent.

$X_2YZ$	Structure	$m^{\text{Co}^I}$ ( $\mu_B$ )	$m^{\text{Co}^{II}}$ ( $\mu_B$ )	$m^{\text{Mn}}$ ( $\mu_B$ )	$m^Z$ ( $\mu_B$ )	$m^{\text{f.u.}}$ ( $\mu_B$ )	$Z_t$
$\text{Co}_2\text{MnSc}$	$L2_1$	0.82	0.82	3.12	−0.44	4.31	
	$XA$	1.23	1.56	2.95	−0.42	5.31	
$\text{Co}_2\text{MnY}$	$L2_1$	0.85	0.85	3.46	−0.35	4.82	28
	$XA$	1.19	1.50	3.16	−0.36	5.50	
$\text{Co}_2\text{MnLu}$	$L2_1$	0.76	0.76	3.27	−0.30	4.49	
	$XA$	1.14	1.51	3.01	−0.29	5.38	
$\text{Co}_2\text{MnTi}$	$L2_1$	1.05	1.05	3.23	−0.45	4.87	
	$XA$	1.20	1.61	2.45	−0.65	4.61	
$\text{Co}_2\text{MnZr}$	$L2_1$	0.98	0.98	3.47	−0.37	5.07	29
	$XA$	1.03	1.54	2.60	−0.49	4.68	
$\text{Co}_2\text{MnHf}$	$L2_1$	0.98	0.98	3.43	−0.35	5.03	
	$XA$	0.98	1.55	2.48	−0.39	4.62	
$\text{Co}_2\text{MnV}$	$L2_1$	1.15	1.15	3.07	0.25	5.62	
	$XA$	1.12	1.52	2.14	−0.93	3.85	
$\text{Co}_2\text{MnNb}$	$L2_1$	1.22	1.22	3.50	−0.13	5.80	30
	$XA$	0.88	1.46	2.25	−0.52	4.07	
$\text{Co}_2\text{MnTa}$	$L2_1$	1.19	1.19	3.44	−0.13	5.70	
	$XA$	0.76	1.50	2.04	−0.44	3.86	
$\text{Co}_2\text{MnCr}$	$L2_1$	1.23	1.23	2.95	1.32	6.73	
	$XA$	0.76	1.53	2.32	−1.71	2.89	
$\text{Co}_2\text{MnMo}$	$L2_1$	1.40	1.40	3.38	0.20	6.37	31
	$XA$	−0.05	1.34	2.04	−0.47	2.85	
$\text{Co}_2\text{MnW}$	$L2_1$	1.39	1.39	3.41	0.11	6.29	
	$XA$	−0.01	1.42	1.83	−0.37	2.87	

As evident from the discussion above on spin magnetic moments, only the  $\text{Co}_2\text{MnZ}$  compounds adhere to the Slater–Pauling rule, as outlined in Ref. [41]. In these compounds, there is no true gap, and the Fermi level consistently crosses a spin-down energy band. When the total spin magnetic moment approaches the integer value predicted by the Slater–Pauling rule described in Ref. [41], the spin-down gap can be attributed to the hybridization of the  $d$  valence orbitals of neighboring atoms. If  $M_t$  represents the total spin magnetic moment per formula unit, and  $Z_t - 24$  is the total number of valence electrons per unit cell, then the Slater–Pauling rule becomes  $M_t = Z_t - 24$ . This rule links the electronic and magnetic properties of ideal half-metals.



**Table 4.** These data are similar to Table 3 for all compounds under study assuming only the  $L2_1$  lattice structure.

$L2_1$	$m^{Co,Rh,Ru}$ ( $\mu_B$ )	$m^{Mn}$ ( $\mu_B$ )	$m^Z$ ( $\mu_B$ )	$m^{f.u.}$ ( $\mu_B$ )	$Z_t$
Co <sub>2</sub> MnSc	0.82	3.12	−0.44	4.31	28
Co <sub>2</sub> MnY	0.85	3.46	−0.35	4.82	
Co <sub>2</sub> MnLu	0.76	3.27	−0.30	4.49	
Rh <sub>2</sub> MnSc	0.28	3.96	−0.22	4.31	
Rh <sub>2</sub> MnY	0.25	4.17	−0.13	4.53	
Rh <sub>2</sub> MnLu	0.39	4.07	−0.12	4.42	
Ru <sub>2</sub> MnSc	−0.20	3.10	−0.09	2.61	
Ru <sub>2</sub> MnY	−0.15	3.60	−0.02	3.28	
Ru <sub>2</sub> MnLu	−0.19	3.41	−0.01	3.03	
Co <sub>2</sub> MnTi	1.05	3.23	−0.45	4.87	29
Co <sub>2</sub> MnZr	0.98	3.47	−0.37	5.07	
Co <sub>2</sub> MnHf	0.98	3.43	−0.35	5.03	
Rh <sub>2</sub> MnTi	0.33	4.07	0.05	4.78	
Rh <sub>2</sub> MnZr	0.28	4.20	−0.03	4.72	
Rh <sub>2</sub> MnHf	0.28	4.17	−0.03	4.71	
Ru <sub>2</sub> MnTi	−0.01	3.33	−0.01	3.28	
Ru <sub>2</sub> MnZr	0.01	3.63	−0.04	3.62	
Ru <sub>2</sub> MnHf	−0.00	3.55	−0.06	3.49	
Co <sub>2</sub> MnV	1.15	3.07	0.25	5.62	30
Co <sub>2</sub> MnNb	1.22	3.50	−0.13	5.80	
Co <sub>2</sub> MnTa	1.19	3.44	−0.13	5.70	
Rh <sub>2</sub> MnV	0.33	3.90	0.14	4.70	
Rh <sub>2</sub> MnNb	0.19	4.05	−0.05	4.39	
Rh <sub>2</sub> MnTa	0.17	4.04	−0.04	4.35	
Ru <sub>2</sub> MnV	0.07	3.44	0.44	4.01	
Ru <sub>2</sub> MnNb	0.18	3.70	0.01	4.07	
Ru <sub>2</sub> MnTa	0.19	3.71	−0.02	4.06	
Co <sub>2</sub> MnCr	1.23	2.95	1.32	6.73	31
Co <sub>2</sub> MnMo	1.40	3.38	0.20	6.37	
Co <sub>2</sub> MnW	1.39	3.41	0.11	6.29	
Rh <sub>2</sub> MnCr	0.26	3.79	2.85	7.17	
Rh <sub>2</sub> MnMo	0.09	3.92	−0.50	3.59	
Rh <sub>2</sub> MnW	0.10	3.90	−0.27	3.83	
Ru <sub>2</sub> MnCr	−0.08	3.32	1.89	5.05	
Ru <sub>2</sub> MnMo	0.35	3.75	0.03	4.49	
Ru <sub>2</sub> MnW	0.39	3.85	0.01	4.63	

In the lower panel of Figure 4, we plot the total spin magnetic moment for Co<sub>2</sub>MnZ compounds as a function of the total number of valence electrons when Z is a 3d, 4d, or 5d transition metal atom. In all cases, the total spin magnetic moments closely match the values predicted by the Slater–Pauling rule, and the hybridization scheme discussed in Ref. [41] applies. However, when Ru substitutes for Co, the total spin magnetic moment for isovalent compounds is constantly lower than the value predicted by the Slater–Pauling rule, as shown in the upper panel of Figure 4. For Rh compounds (middle panel of Figure 4), the behavior for early transition metal atoms resembles that of Co-based compounds, while for heavier transition metals, it mirrors the behavior of Ru compounds, with the exception of Rh<sub>2</sub>MnCr. As mentioned in the previous section, there is a spin-down pseudogap in all Rh and Ru compounds (see Figure 1), and in most cases, the Fermi level lies within this pseudogap. When compared to the schematic minority spin band structure in Figure 7 of Ref. [41], for compounds that deviate from the Slater–Pauling rule, a band just above the Fermi level in the Co<sub>2</sub>-compounds becomes occupied, leading to a narrower pseudogap and a smaller spin magnetic moment than the ideal value.

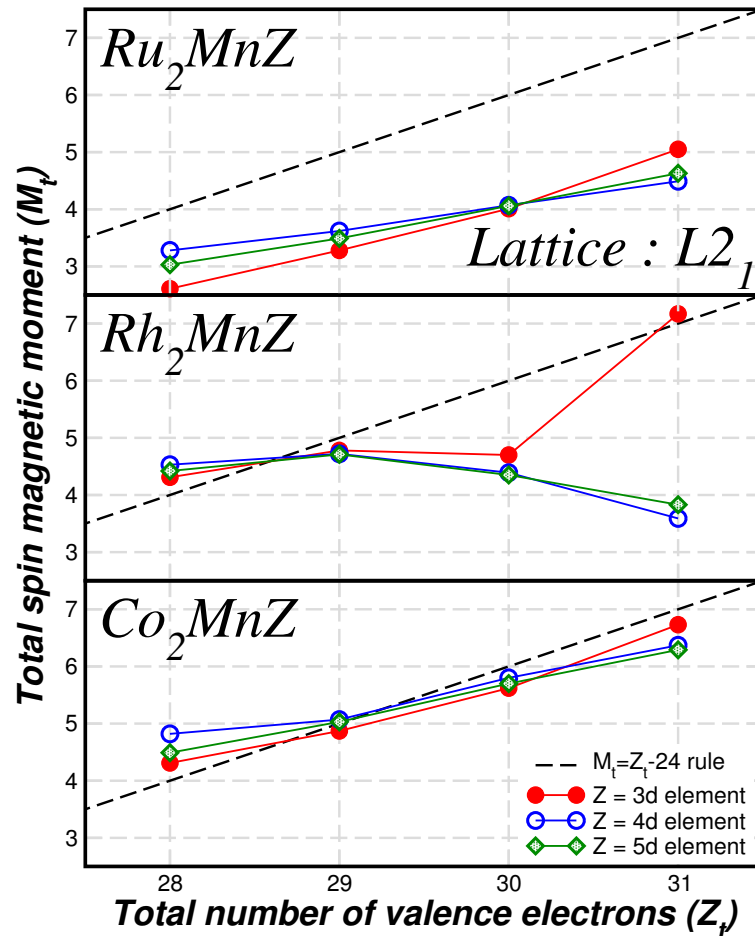


**Figure 4.** Ab initio calculated total spin magnetic moments,  $M_t$ , in  $\mu_B$  as a function of the total number of valence electrons,  $Z_t$ , in the primitive unit cell for the studied compounds at their equilibrium lattice constant assuming the  $L2_1$  lattice structure. The dashed line represents the  $M_t = Z_t - 24$  Slater–Pauling rule.

#### 4. Summary and Conclusions

All- $d$  metallic Heusler compounds have been recently proposed as promising materials for nanoelectronic devices, also encompassing magnetic materials, but studies have been limited to cases where only  $3d$  transition metal atoms are present. Using ab initio electronic structure calculations, we have introduced a new class of magnetic Heusler compounds, consisting solely of  $3d$ ,  $4d$ , and  $5d$  metallic atoms and characterized by high spin magnetic moments. These compounds have the chemical formula  $X_2MnZ$ , where  $X$  is Co, Rh, or Ru, and  $Z$  is a transition metal atom such that the valence order is  $Co(Rh, Ru) > Mn > Z$ . Most of these compounds exhibit a region of very low density of minority-spin states at the Fermi level when crystallized in the  $L2_1$  lattice structure. For Co-based compounds, the total spin magnetic moments per formula unit are close to integer values and follow the Slater–Pauling rule. In the Ru-based compounds, the  $5d$  valence states result in total spin magnetic moments that are about  $2 \mu_B$  lower than those of the corresponding Co-based compounds. Rh-based compounds show magnetic properties similar to Co-based compounds for lighter  $Z$  elements and to Ru-based compounds for heavier  $Z$  elements. Our results further indicate that the electronic and magnetic properties are only minimally influenced by the specific choice of the  $Z$  element within the same column of the periodic table, with the exception of the  $Rh_2MnCr$  and  $Rh_2MnMo(W)$  compounds.

We expect that our findings will encourage additional theoretical and experimental research on these compounds, which have promising potential for applications in spintronics and magnetoelectronics.

**Author Contributions:** M.T., E.Ş. and I.G. have equally contributed to this work. All authors have read and agreed to the published version of the manuscript.

**Funding:** This research received no external funding.

**Data Availability Statement:** The data presented in this study are available on request from the corresponding author.

**Conflicts of Interest:** The authors declare no conflicts of interest.

### Abbreviations

The following abbreviations are used in this manuscript:

DOS	Density of states
f.u.	Formula unit
FPLO	Full-potential nonorthogonal local-orbital minimum-basis band structure approach
GGA	Generalized gradient approximation
PBE	Perdew–Burke–Ernzerhof

### References

1. Heusler, F. Über magnetische manganlegierungen. *Verh. Dtsch. Phys. Ges.* **1903**, *12*, 219.
2. Heusler, F.; Take, E. The nature of the Heusler alloys. *Phys. Z.* **1912**, *13*, 897. [[CrossRef](#)]
3. Webster, P.J.; Ziebeck, K.R.A. Alloys and Compounds of *d*-Elements with Main Group Elements. Part 2. In *Landolt-Börnstein, New Series, Group III*; Wijn, H.R.J., Ed.; Springer: Berlin/Heidelberg, Germany, 1988; Volume 19c, pp. 75–184.
4. Ziebeck, K.R.A.; Neumann, K.-U. Magnetic Properties of Metals. In *Landolt-Börnstein, New Series, Group III*; Wijn, H.R.J., Ed.; Springer: Berlin/Heidelberg, Germany, 2001; Volume 32/c, pp. 64–414.
5. Graf, T.; Felser, C.; Parkin, S.S.P. Simple rules for the understanding of Heusler compounds. *Prog. Solid State Chem.* **2011**, *39*, 1. [[CrossRef](#)]
6. Katsnelson, M.I.; Irkhin, V.Y.; Chioncel, L.; Lichtenstein, A.I.; de Groot, R.A. Half-metallic ferromagnets: From band structure to many-body effects. *Rev. Mod. Phys.* **2008**, *80*, 315. [[CrossRef](#)]
7. Galanakis, I. Slater–Pauling Behavior in Half-Metallic Heusler Compounds. *Nanomaterials* **2023**, *13*, 2010. [[CrossRef](#)] [[PubMed](#)]
8. Hirohata, A.; Takanashi, K. Perspectives of Heusler compounds. *J. Phys. D Appl. Phys.* **2014**, *47*, 193001. [[CrossRef](#)]
9. Half-Metallic Alloys: Fundamentals and Applications. In *Lectures Notes in Physics*; Galanakis, I., Dederichs, P.H., Eds.; Springer: Berlin/Heidelberg, Germany, 2005; Volume 676.
10. Felser, C.; Fecher, G.H. (Eds.) *Spintronics. From Materials to Devices*; Springer: Berlin/Heidelberg, Germany, 2013.
11. Fong, C.Y.; Pask, J.E.; Yang, L.H. (Eds.) Half-metallic Materials and Their Properties. In *Series on Materials for Engineering*; Imperial College Press: London, UK, 2013; Volume 2.
12. Felser, C.; Hirohata, A. (Eds.). Heusler Alloys. Properties, Growth, Applications. In *Springer Series in Materials Science*; Springer International Publishing: Berlin/Heidelberg, Germany, 2018; Volume 222.
13. Gillessen, M.; Dronskowski, R. A combinatorial study of full Heusler alloys by first-principles computational methods. *J. Comput. Chem.* **2009**, *30*, 1290. [[CrossRef](#)]
14. Gillessen, M.; Dronskowski, R. A combinatorial study of inverse Heusler alloys by first-principles computational methods. *J. Comput. Chem.* **2010**, *31*, 612. [[CrossRef](#)]
15. Ma, J.; Hegde, V.I.; Munira, K.; Xie, Y.; Keshavarz, S.; Mildebrath, D.T.; Wolverton, C.; Ghosh, A.W.; Butler, W.H. Computational investigation of half-Heusler compounds for spintronics applications. *Phys. Rev. B* **2017**, *95*, 024411. [[CrossRef](#)]
16. Ma, J.; He, J.; Mazumdar, D.; Munira, K.; Keshavarz, S.; Lovorn, T.; Wolverton, C.; Ghosh, A.W.; Butler, W.H. Computational investigation of inverse Heusler compounds for spintronics applications. *Phys. Rev. B* **2018**, *98*, 094410. [[CrossRef](#)]
17. Sanvito, S.; Oses, C.; Xue, J.; Tiwari, A.; Zic, M.; Archer, T.; Tozman, P.; Venkatesan, M.; Coey, M.; Curtarolo, S. Accelerated discovery of new magnets in the Heusler alloy family. *Sci. Adv.* **2017**, *3*, e1602241. [[CrossRef](#)]
18. Faleev, S.V.; Ferrante, Y.; Jeong, J.; Samant, M.G.; Jones, B.; Parkin, S.S.P. Unified explanation of chemical ordering, the Slater–Pauling rule, and half-metallicity in full Heusler compounds. *Phys. Rev. B* **2017**, *95*, 045140. [[CrossRef](#)]
19. Faleev, S.V.; Ferrante, Y.; Jeong, J.; Samant, M.G.; Jones, B.; Parkin, S.S.P. Origin of the Tetragonal Ground State of Heusler Compounds. *Phys. Appl.* **2017**, *7*, 034022. [[CrossRef](#)]
20. Faleev, S.V.; Ferrante, Y.; Jeong, J.; Samant, M.G.; Jones, B.; Parkin, S.S.P. Heusler compounds with perpendicular magnetic anisotropy and large tunneling magnetoresistance. *Phys. Rev. Mater.* **2017**, *1*, 024402. [[CrossRef](#)]
21. Oliynyk, A.O.; Antono, E.; Sparks, T.D.; Ghadbeigi, L.; Gaultois, M.W.; Meredig, B.; Mar, A. High-Throughput Machine-Learning-Driven Synthesis of Full-Heusler Compounds. *Chem. Mater.* **2016**, *28*, 7324. [[CrossRef](#)]
22. Ni, Z.; Ma, Y.; Liu, X.; Luo, H.; Liu, H.; Meng, F. Electronic structure, magnetic properties and martensitic transformation in all-d-metal Heusler alloys. *J. Magn. Magn. Mater.* **2018**, *451*, 721. [[CrossRef](#)]

23. Wei, Z.Y.; Liu, E.K.; Li, Y.; Han, X.L.; Du, Z.W.; Luo, H.Z.; Liu, G.D.; Xi, X.K.; Zhang, H.W.; Wang, W.H.; et al. Magnetostructural martensitic transformations with large volume changes and magneto-strains in all-d-metal Heusler alloys. *Appl. Phys. Lett.* **2016**, *109*, 071904. [CrossRef]
24. Wei, Z.Y.; Liu, E.K.; Chen, J.H.; Li, Y.; Liu, G.D.; Luo, H.Z.; Xi, X.K.; Zhang, H.W.; Wang, W.H.; Wu, G.H. Realization of multifunctional shape-memory ferromagnets in all-d-metal Heusler phases. *Appl. Phys. Lett.* **2015**, *107*, 022406. [CrossRef]
25. Ni, Z.; Guo, X.; Liu, X.; Jiao, Y.; Meng, F.; Luo, H. Understanding the magnetic structural transition in all-d-metal Heusler alloy  $Mn_2Ni_{1.25}Co_{0.25}Ti_{0.5}$ . *J. Alloys Compd.* **2019**, *775*, 427. [CrossRef]
26. Samanta, S.; Ghosh, S.; Mandal, K. Observation of giant exchange bias effect in Ni–Mn–Ti all-d-metal Heusler alloy. *J. Phys. Condens. Matter* **2022**, *34*, 105801. [CrossRef]
27. Aznar, A.; Gràcia-Condal, A.; Planes, A.; Lloveras, P.; Barrio, M.; Tamarit, J.-L.; Xiong, W.; Cong, D.; Popescu, C.; Manosa, L. Giant barocaloric effect in all-d-metal Heusler shape memory alloys. *Phys. Rev. Mater.* **2019**, *3*, 044406. [CrossRef]
28. Samanta, S.; Ghosh, S.; Chatterjee, S.; Mandal, K. Large magnetocaloric effect and magnetoresistance in Fe-Co doped  $Ni_{50-x}(FeCo)_xNn_{37}Ti_{13}$  all-d-metal Heusler alloys. *J. Alloys Compd.* **2022**, *910*, 164929. [CrossRef]
29. Samanta, S.; Chatterjee, S.; Ghosh, S.; Mandal, K. Large reversible magnetocaloric effect and magnetoresistance by improving crystallographic compatibility condition in Ni(Co)- Mn-Ti all-d-metal Heusler alloys. *Phys. Rev. Mater.* **2022**, *6*, 094411. [CrossRef]
30. Shena, J.; Zeng, Q.; Zhang, H.; Xi, X.; Liu, E.; Wang, W.; Wu, G. Atomic configuration, unusual lattice constant change, and tunable ferromagnetism in all-d-metal Heusler alloys  $Fe_2CrV-FeCr_2V$ . *J. Magn. Magn. Mater.* **2019**, *492*, 165661. [CrossRef]
31. Mert, G. Magnetic phase transitions of all-d metal Heusler type model. *J. Alloy. Compd.* **2020**, *819*, 153299. [CrossRef]
32. Tanzim, M.F.; Fortunato, N.; Samathrakris, I.; Xie, R.; Opahle, I.; Gutfleisch, O.; Zhang, H. Giant Anomalous Hall and Nernst Conductivities in Magnetic All-d Metal Heusler Alloys. *Adv. Funct. Mater.* **2023**, *33*, 2214967. [CrossRef]
33. de Paula, V.G.; Reis, M.S. All-d-Metal Full Heusler Alloys: A Novel Class of Functional Materials. *Chem. Mater.* **2021**, *33*, 5483. [CrossRef]
34. Marathe, M.; Herper, H.C. Exploration of all-3d Heusler alloys for permanent magnets: An ab initio based high-throughput study. *Phys. Rev. B* **2023**, *107*, 174402. [CrossRef]
35. Nia, S.; Khenchoul, S.; Lefkaier, I.K.; Lagoun, B. DFT-based investigation of the structural, magnetic, electronic, half-metallicity and elastic properties in the all-d heusler compounds: The case of  $Co_2VZn$  and  $CoVZn$ . *Eur. Phys. J. B* **2021**, *94*, 118. [CrossRef]
36. Jin, T.; Jung, Y. Classifying Intermetallic Tetragonal Phase of All-d-Metal Heusler Alloys for Catalysis Applications. *Today Catal.* **2022**, *65*, 208. [CrossRef]
37. Zeng, Q.; Shen, J.; Zhang, H.; Chen, J.; Ding, B.; Xi, X.; Liu, E.; Wang, W.; Wu, G. Electronic behaviors during martensitic transformations in all-d-metal Heusler alloys. *J. Phys. Condens. Matter* **2019**, *31*, 425401. [CrossRef] [PubMed]
38. Fortunato, N.M.; Taubel, A.; Marmodoro, A.; Pfeuffer, L.; Ophale, I.; Ebert, H.; Gutfleisch, O.; Zhang, H. High-Throughput Design of Magnetocaloric Materials for Energy Applications: MMX alloys. *Adv. Sci.* **2023**, *10*, 2206772. [CrossRef]
39. Fortunato, N.M.; Li, X.; Schöpnecker, S.; Xie, R.; Taubel, A.; Scheibel, F.; Opahle, I.; Gutfleisch, O.; Zhang, H. High-Throughput Screening of All-d-Metal Heusler Alloys for Magnetocaloric Applications. *Chem. Mater.* **2024**, *3*, 6765. [CrossRef]
40. Özdoğan, K.; Maznichenko, I.V.; Ostanin, S.; Şaşıoğlu, E.; Ernst, A.; Mertig, I.; Galanakis, I. High spin polarization in all-3d-metallic Heusler compounds: The case of  $Fe_2CrZ$  and  $Co_2CrZ$  ( $Z = Sc, Ti, V$ ). *J. Phys. D Appl. Phys.* **2019**, *52*, 205003. Corrigendum **2024**, *57*, 049501. [CrossRef]
41. Tas, M.; Özdoğan, K.; Şaşıoğlu, E.; Galanakis, I. High Spin Magnetic Moments in All-3d-Metallic Co-Based Full Heusler Compounds. *Materials* **2023**, *16*, 7543. [CrossRef]
42. Koepnick, K.; Eschrig, H. Full-potential nonorthogonal local-orbital minimum-basis band-structure scheme. *Phys. Rev. B* **1999**, *59*, 1743. [CrossRef]
43. Kopernik, K. Full Potential Local Orbital Minimum Basis Bandstructure Scheme User's Manual. Available online: <http://www.fplo.de/> (accessed on 1 September 2024).
44. Perdew, J.P.; Burke, K.; Ernzerhof, M. Generalized Gradient Approximation Made Simple. *Phys. Rev. Lett.* **1996**, *77*, 3865. [CrossRef]
45. Galanakis, I.; Dederichs, P.H.; Papanikolaou, N. Origin and Properties of the Gap in the Half-Ferromagnetic Heusler Alloys. *Phys. Rev. B* **2002**, *66*, 134428. [CrossRef]
46. Galanakis, I.; Dederichs, P.H.; Papanikolaou, N. Slater-Pauling Behavior and Origin of the Half-Metallicity of the Full-Heusler Alloys. *Phys. Rev. B* **2002**, *66*, 174429. [CrossRef]
47. Monkhorst, H.J.; Pack, J.D. Special points for Brillouin-zone integrations. *Phys. Rev. B* **1976**, *13*, 5188. [CrossRef]
48. Available online: <https://oqmd.org> (accessed on 1 September 2024).
49. Saal, J.E.; Kirklin, S.; Aykol, M.; Meredig, B.; Wolverton, C. Materials Design and Discovery with High-Throughput Density Functional Theory: The Open Quantum Materials Database (OQMD). *JOM* **2013**, *65*, 1501. [CrossRef]
50. Kirklin, S.; Saal, J.E.; Meredig, B.; Thompson, A.; Doak, J.W.; Aykol, M.; Rühl, S.; Wolverton, C. The Open Quantum Materials Database (OQMD): Assessing the accuracy of DFT formation energies. *npj Comput. Mater.* **2015**, *1*, 15010. [CrossRef]

**Disclaimer/Publisher's Note:** The statements, opinions and data contained in all publications are solely those of the individual author(s) and contributor(s) and not of MDPI and/or the editor(s). MDPI and/or the editor(s) disclaim responsibility for any injury to people or property resulting from any ideas, methods, instructions or products referred to in the content.